Journal of Materials Chemistry C

Accepted Manuscript

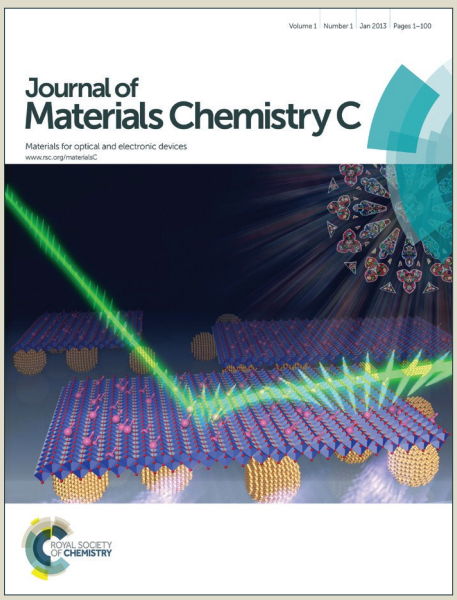

ROYAL SOCIETY OF CHEMISTRY

www.rsc.org/materialsC

Highly Stretchable and Sensitive Piezoresistive Carbon Nanotube /Elastomeric Triisocyanate-Crosslinked Polytetrahydrofuran Nanocomposites

Yunming Wang[§a], Hongyi Mi[§b], Qifeng Zheng[a], Huilong Zhang[b], Zhenqiang Ma[*b], and Shaoqin Gong[1*]

[a]Department of Biomedical Engineering, Wisconsin Institute for Discovery, and Materials Science Program, University of Wisconsin–Madison, Madison, WI 53706, USA

[b]Department of Electrical and Computer Engineering, University of Wisconsin–Madison, WI 53706, USA

[§]These authors contributed equally to this work.

*Corresponding authors: mazq@engr.wisc.edu, Tel: +1-608-261-1095;

sgong@engr.wisc.edu, Tel: +1-608-316-4311.

[†]Electronic supplementary information (ESI) available: material characterizations, measurement setup and mathematic equation analysis. See DOI: 10.1029/x0xx00000x

Abstract

Piezoresistive polymer nanocomposites are highly desirable for flexible mechanical sensing applications. In this study, a family of multi-walled carbon nanotube (CNT)/elastomeric triisocyanate-crosslinked polytetrahydrofuran (ETC-PTHF) nanocomposites that are highly stretchable and highly sensitive to mechanical stimuli were designed, synthesized, and characterized. The CNTs in the CNT/ETC-PTHF nanocomposites were initially dispersed in the ETC-PTHF matrix uniformly, leading to a relatively high electrical conductivity. Upon stretching, both the degree of CNT alignment along the stretching direction and the degree of PTHF crystallinity increased consistently with the tensile strain. The strain-induced microstructure change adversely affected the CNT conducting pathways thereby causing a reduction in the electrical conductivity of the nanocomposites. For instance, the electrical conductivity of the 15 wt.% CNT/ETC-PTHF nanocomposites changed approximately 7.3%, 29.2%, 19.76, 169.2 and 1291 times when the tensile strain was 1%, 5%, 50%, 250%, and 500%, respectively. The nanocomposite film was able to detect a mechanical stimulus (poking) weaker than the landing force of a mosquito. Furthermore, the nanocomposite film demonstrated rapid and highly sensitive responses to a continuous finger motion. These new piezoresistive CNT/ETC-PTHF nanocomposites possess a number of desirable characteristics including ease of fabrication, low cost, and high sensitivity, thereby making them very promising candidates for applications in electronic skins, electronic textiles, and biomedical detectors.

Keywords: Polymer nanocomposites; carbon nanotubes; piezoresistive**;** phase change materials; human motion detection

1. Introduction

Flexible piezoresistive polymer nanocomposites exhibiting high sensitivity to mechanical stimuli can be potentially used to make sensory skins,[1-3] wearable health monitors,[4, 5] electronic textiles,[6, 7] and biomedical detectors[8] with high durability for body movements and deformations.[9-11] The irreplaceable advantages of flexible piezoresistive polymer nanocomposites, compared with their traditional rigid counterparts, include ease of fabrication, high flexibility, excellent impact resistance, light weight, and low cost.[12, 13] During the past few years, significant efforts have been dedicated to developing flexible, stretchable, and sensitive piezoresistive nanocomposites.[8, 9, 14, 15] In particular, piezoresistive nanocomposites employing[11, 16, 17] carbon nanoparticles, including graphene and carbon nanotubes, have attracted a great deal of interest due to their unique electrical and mechanical properties as well as their relatively low cost.[3, 11, 15, 16, 3, 18, 19] The performance of piezoresistive nanocomposites is determined by a number of factors including the formulation, processes, and resulting microstructures.[8, 9, 11, 16, 17] Although great strides have been made in the area of carbon nanoparticle-based piezoresistive nanocomposites, there still exists certain challenges. For instance, highly sensitive strain sensors made of graphene nanocomposites exhibited relatively low stretchability (maximum $\varepsilon \leqslant 100\%$).[20] Similarly, highly stretchable strain sensors made from carbon nanotube (CNT)/polymer (e.g.,

PU or silicone rubber) nanocomposites exhibited relatively low maximum gauge factors (GFs, GF = (ΔR/R)/ε, GF < 120) and hence relatively low sensitivity.[21, 22] Both low stretchability and low sensitivity can severely limit the application of such piezoresistive materials for mechanical sensing.

In order to obtain flexible piezoresistive materials with a high sensitivity and high stretchability, we designed and synthesized a family of nanocomposites composed of multi-walled carbon nanotubes (CNTs) and a novel elastomeric triisocyanate-crosslinked polytetrahydrofuran (ETC-PTHF) (i.e., CNT/ ETC-PTHF nanocomposites). The electrically conductive CNTs were initially uniformly dispersed in the ETC-PTHF matrix forming an electrical conducting pathway that could be regulated via a mechanical stimulus such as stretching. During the stretching process, the originally randomly distributed CNTs formed a preferential alignment along the stretching direction, while the PTHF component of the ETC-PTHF underwent an amorphous-to-crystalline transition. The strain-induced microstructure change adversely affected the CNT conducting pathways such that the electrical conductivity of the CNT/ETC-PTHF nanocomposites was reduced. These unique characteristics make the highly stretchable CNT/ETC-PTHF nanocomposites very sensitive to mechanical stimuli. For instance, the electrical conductivity of the 15 wt.% nanocomposites changed up to 7.3%, 29.2%, 19.76, 169.2 and 1291 times when subjected to 1%, 5%, 50%, 250%, and 500% stretching strain, respectively. The corresponding gauge factors of the 15 wt.% CNT/ETC-PTHF nanocomposites under 1%, 5%, 50%, 250%, and 500% stretching strain were 10.0, 11.2, 74.6, 839.3

and 8491, respectively. The nanocomposite film was able to detect a mechanical stimulus (poking) weaker than the landing force of a mosquito. Furthermore, the nanocomposite film demonstrated rapid and highly sensitive responses to a continuous finger motion. Compared with previously reported conductive nanofiller/polymer nanocomposites, these novel CNT/ETC-PTHF nanocomposites demonstrate several outstanding features, including ease of fabrication, low cost detection limit, excellent stretchability, and high sensitivity, thereby making them very promising candidates for applications in electronic skins, electronic textiles, and biomedical detectors.

2. Results and Discussion

2.1 Preparation and characterization of the CNT/ETC-PTHF nanocomposites

Highly stretchable and highly sensitive CNT/ETC-PTHF nanocomposite films were prepared by mixing p-methoxyphenyl functionalized CNTs and ETC-PTHF under ultrasonication in a petri dish followed by heating. The ETC-PTHF used in this study was synthesized using di-functional PHTF and tri-functional TTI. The chemical structure of the obtained nanocomposites was confirmed by FTIR analysis (cf. Figure S1). As shown in Fig. 1a, the electrical conductivity of the resulting CNT/ETC-PTHF nanocomposite films increased with the loading content of CNTs (ranging from 5 to 20 wt.%). This expected result confirms that better electrical conducting pathways were formed with more CNTs in the ETC-PTHF matrix. To investigate the response

of the CNT/ETC-PTHF nanocomposites on mechanical stimuli, the electrical conductivity of the nanocomposite films subjected to a wide range of tensile strains were measured. Fig. 1b shows the electrical conductance changes (G/G_0) of the nanocomposite films with different CNT loading levels (i.e., 5, 10, 15, and 20 wt.%) during the stretching processes. The electrical conductance of these nanocomposites decreased dramatically when the tensile strain increased. For instance, the electrical conductance of the 15 wt.% CNT/ETC-PTHF nanocomposite decreased 10.1%, 35.8%, 38.31, 2099 and 42455 times corresponding to a strain of 1%, 5%, 50%, 250%, and 500%, respectively. In contrast, the gauge factors of these nanocomposites increased with the tensile strain as shown in Fig. 1c. For instance, the gauge factors of the 15 wt.% CNT/ETC-PTHF nanocomposite were 10.0, 11.2, 74.6, 839.3 and 8491 corresponding to a strain of 1%, 5%, 50%, 250%, and 500%, respectively. In order to accurately calculate the electrical conductivity changes of the nanocomposite films in response to the varying tensile strains during the stretching process, the Poisson's ratio of the nanocomposite films was calculated by measuring the thickness and width changes induced by the longitudinal tensile strain. The electrical conductivity was calculated according to Equation 1 based on the measured electrical data and the Poisson's ratios. Detailed information on the derivation of Equation 1 is provided in the Supporting Information. The equation for the conductivity (σ) of the stretchable CNT/ETC-PTHF nanocomposites is as follows,[23]

$$\sigma = G\frac{L_0(1+\varepsilon_L)}{W_0T_0(1-\varepsilon_L\upsilon_{thickness})(1-\varepsilon_L\upsilon_{width})} \quad (1)$$

where G is the conductance of the stretchable CNT/ETC-PTHF nanocomposite; ε_L is the longitudinal direction strain; and L_0, W_0, and T_0 are the initial length, thickness, and width of the film, respectively. The parameter $\upsilon_{thickness}$ is the Poisson's ratio measured by tracking the thickness change, and υ_{width} is the Poisson's ratio measured by tracking the width change. As shown in Fig. S3a, the Poisson's ratios decreased with an increasing tensile strain.[24] Similar to the electrical conductance changes shown in Fig. 1b, the electrical conductivities of the nanocomposite films with different CNT loading levels also decreased with increasing tensile strains (cf. Fig. 1d). For example, the decrease of electrical conductivity for the 15 wt.% nanocomposite was 7.3%, 29.2%, 19.76, 169.2 and 1291 times under 1%, 5%, 50%, 250%, and 500% strain, respectively. Additionally, while the magnitude of changes in the electrical conductivity for the CNT/ETC-PTHF did not vary drastically for the nanocomposites with 5, 10, and 15 wt.% CNTs, particularly when the strain was below 300%, the magnitude of changes in the electrical conductivity for the CNT/ETC-PTHF with 20 wt.% CNTs was consistently lower than the nanocomposites with lower CNT loading levels. This was likely due to the fact that numerous CNT conducting pathways were formed at high CNT loading levels (e.g., 20 wt.%). Therefore, the strain-induced microstructure changes, including the CNT alignment and the formation of PTHF crystallites, did not drastically damage the overall CNT conductive pathway.

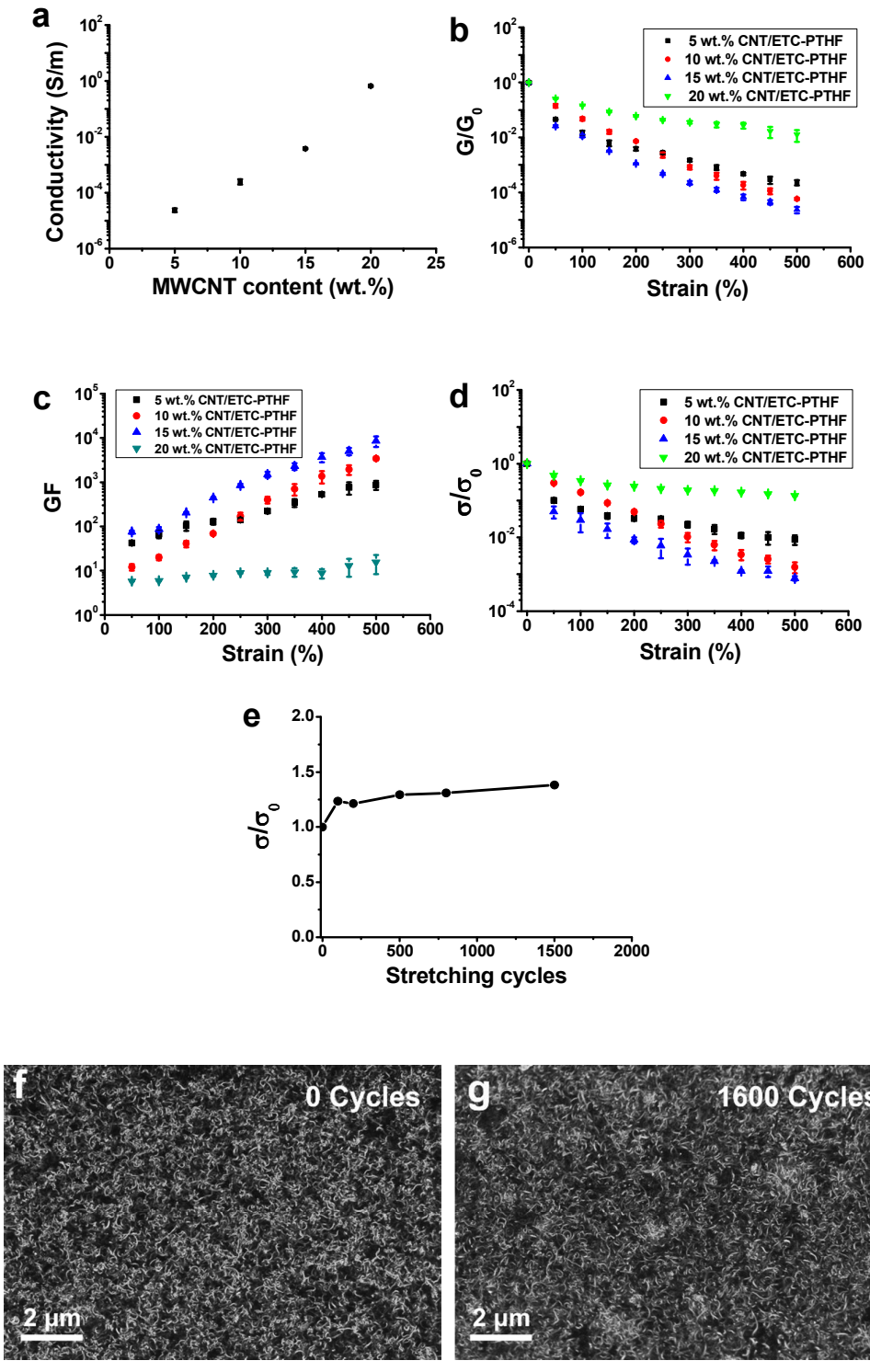

Fig. 1 (a) Dependence of the initial electrical conductivity on the CNT loading content; (b) The change in electrical conductance of the CNT/ETC-PTHF

nanocomposite films as a function of tensile strain; (c) The gauge factors of the CNT/ETC-PTHF nanocomposite films as a function of tensile strain; (d) The change in electrical conductivity of the CNT/ETC-PTHF nanocomposite films as a function of tensile strain; (e) The change in electrical conductivity (σ/σ_0) of the 15 wt.% CNT/ETC-PTHF nanocomposite film after recurrent stretching cycles, ε = 10%; (f) The SEM image of the initial 15 wt.% CNT/ETC-PTHF nanocomposite; and (g) The SEM image of the 15 wt.% CNT/ETC-PTHF nanocomposite after 1600 stretching cycles, ε = 10%.

Further experiments were carried out to investigate the long term reliability and durability of the nanocomposites. Fig. 1e shows the electrical conductivity change of the 15 wt.% CNT/ETC-PTHF nanocomposite film as a function of the number of stretching cycles at a tensile strain of 10%. It was observed that the electrical conductivity of the nanocomposite film increased slightly within the first 100 cycles, and then remained nearly unchanged during the subsequent 1500 cycles. Overall, the electrical conductivity of the nanocomposite film measured at 0% strain only increased by 38% after 1600 stretching cycles. The remarkable cycling stability exhibited by the nanocomposite films with excellent stretchability and sensitivity to mechanical stimuli will certainly be beneficial for various applications. The increase in electrical conductivity during the cyclic test can be likely attributed to a slight change in the connectivity of the electrically conductive CNT network. Scanning electron microscopy (SEM) was used to examine the influence of the cyclic stretch on the microstructure of the CNT/ETC-PTHF nanocomposites. As shown in Figs. 1f and

g, the microstructure of the nanocomposite films and the CNT distribution did not show obvious changes after 1600 consecutive stretches. Additionally, as shown in Fig. S4, the temperature of the CNT/ETC-PTHF nanocomposite corresponding to 5 wt.% weight loss was 315 ℃, suggesting that the nanocomposite had good thermal stability. The tensile properties of the CNT/ETC-PTHF nanocomposites are shown in Fig. S5 and Table S1. For the CNT/ETC-PTHF nanocomposites, the Young's modulus increased while the tensile strain-at-break decreased with the CNT loading content. The tensile strength-at-break initially increased with the CNT content, but decreased somewhat beyond 15 wt.%. However, overall, the mechanical properties of the CNT/ETC-PTHF nanocomposites were very good. For example, the 15% CNT/ETC-PTHF nanocomposite had a Young's modulus of 4.26 ± 0.11 MPa, tensile strength-at-break of 25.16 ± 1.62 MPa, and tensile strain-at-break of 8.92 ± 1.39 times, suggesting that the CNT/ETC-PTHF nanocomposites had excellent stretchability and flexibility. All of these characteristics make the CNT/ETC-PTHF nanocomposites desirable for practical applications.

In order to study the sensitivity of the CNT/ETC-PTHF nanocomposites, the electrical response at low level strains (from 0 to 50%) for the 15 wt.% CNT/ETC-PTHF nanocomposite were also measured (cf. Fig. 2). The electrical conductance (cf. Fig. 2a) consistently decreased, while the gauge factor (cf. Fig. 2b) consistently increased with an increasing tensile strain. Under 1% and 5% strain, the electrical conductance of the 15 wt.% CNT/ETC-PTHF nanocomposite decreased 10.1% and 35.8%, respectively, with a corresponding

gauge factor of 10.0 and 11.2, respectively. Additionally, based on the calculated Possion's ratio as shown in Fig. S3b, the electrical conductivity of the 15 wt.% CNT/ETC-PTHF nanocomposite decreased 7.6% and 29.2%, respectively, under 1% and 5% strain (cf. Fig. 2c).

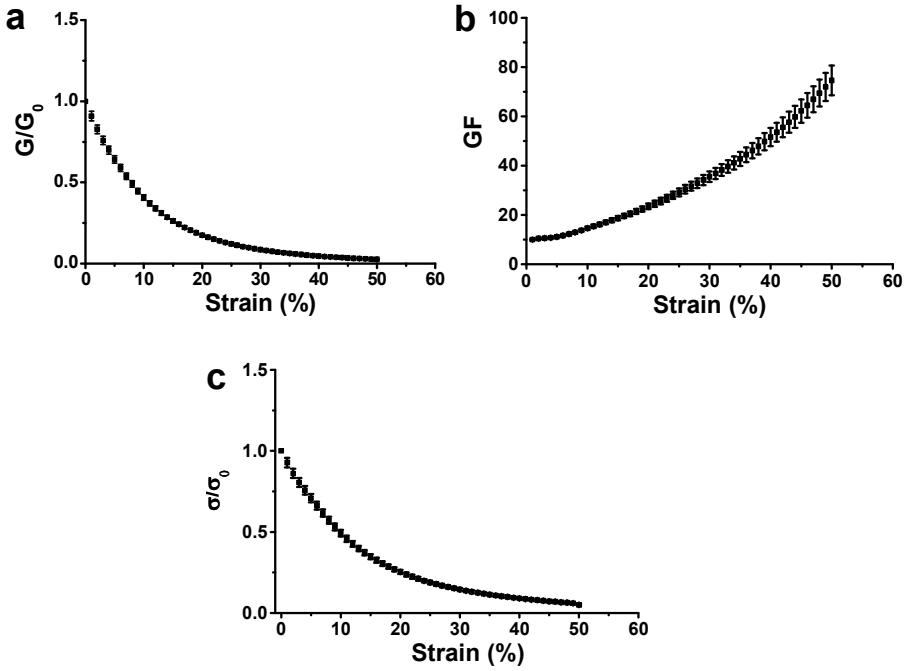

Fig. 2 (a) The change in electrical conductance of the 15 wt.% CNT/ETC-PTHF nanocomposite films as a function of tensile strain ranging from 0 to 50%; (b) The gauge factor of the 15 wt.% CNT/ETC-PTHF nanocomposite films as a function of tensile strain ranging from 0 to 50%. (c) The change in electrical conductivity of the 15 wt.% CNT/ETC-PTHF nanocomposite films as a function of tensile strain ranging from 0 to 50%.

2.2 Study of the piezoresistive mechanism

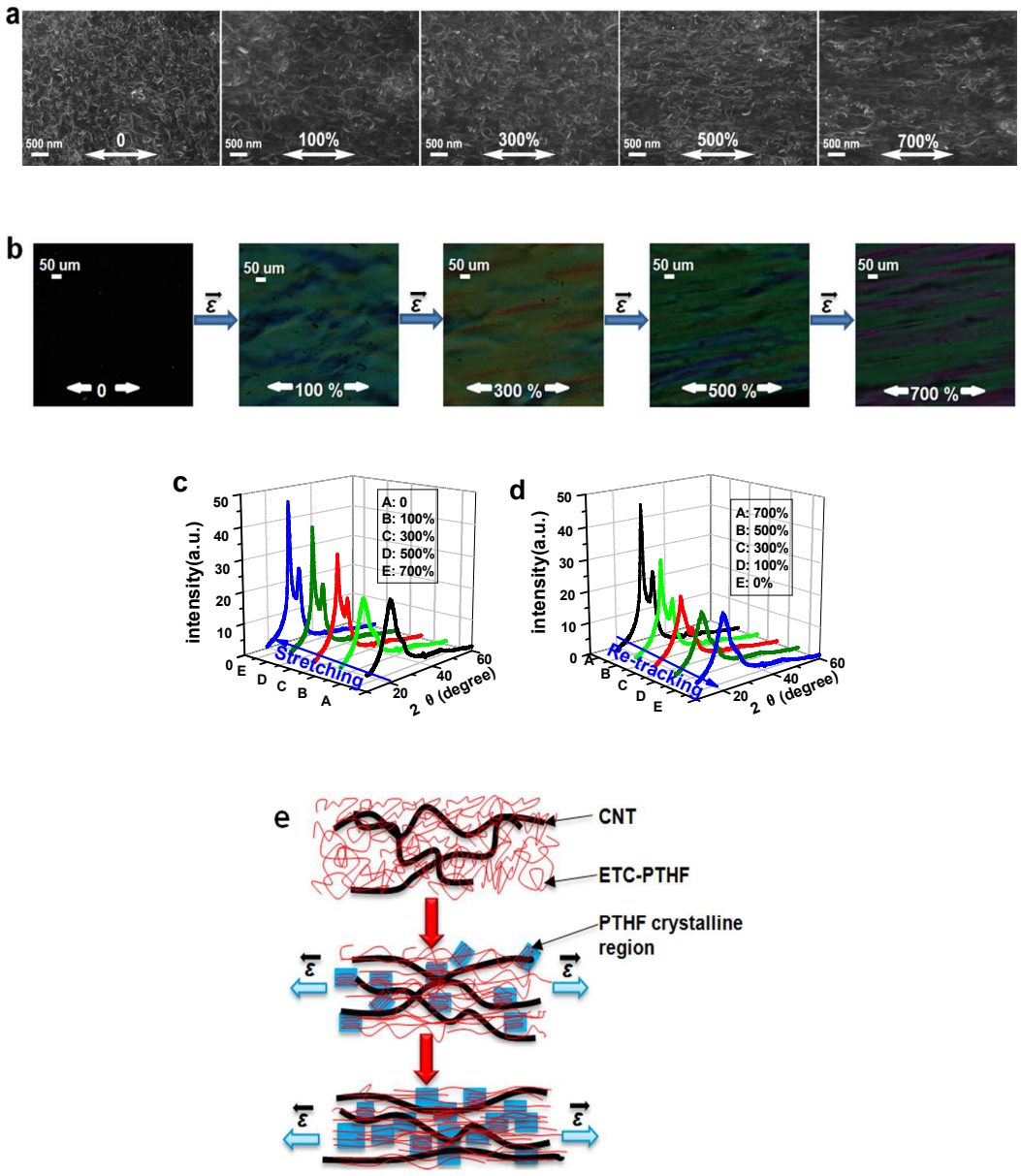

Fig. 3 (a) SEM images of the 15 wt.% CNT/ETC-PTHF nanocomposite film subjected to varying strains: 0%, 100%, 300%, 500%, and 700%; (b) Polarized light microscopy (PLM) images of the ETC-PTHF film under different strains; (c) X-ray diffraction (XRD) curves of the 15 wt.% CNT/ETC-PTHF nanocomposite films during the stretching process; (d) XRD curves of the 15 wt.% CNT/ETC-PTHF nanocomposite during the re-tracking/recovery process; and (e) Conceptual

illustration of the microstructure change of the CNT/ETC-PTHF nanocomposites in response to the stretching and recovery process.

To gain further insight into the electrical conductivity responses to stretching, the microstructure of the CNT/ETC-PTHF nanocomposites under different tensile strains were investigated using SEM. As shown in Fig. 3a, the CNTs in the nanocomposite underwent a rearrangement in response to the tensile strain. Initially, the CNTs, which mostly exhibited a coiled structure, were evenly distributed in the ETC-PTHF matrix. As the tensile strain was applied and increased, the coiled and entangled CNTs started to gradually uncoil, disentangle, and align along the stretching direction. This process could lead to a reduction in the overall electrical connectivity of the CNT network, or a reduction in the efficiency of electron tunneling among the CNTs, and thus a decrease in the electrical conductivity of the nanocomposite film.[25]

Polarized light microscopy (PLM) and XRD were conducted to gain further insight into the mechanism of the piezoresistive effect exhibited by the CNT/ETC-PTHF nanocomposites. Fig. 3b shows the PLM images of the pure ETC-PTHF film collected at room temperature under different tensile strains. The first figure in Fig. 3b is dark, suggesting that the PTHF in the ETC-PTHF was amorphous, which is consistent with the DSC curve measured from room temperature (Fig. S6) showing no PTHF melting peak. This was attributed to the fact that the localized PTHF crystallization temperature in ETC-PTHF under zero strain was around –6.7°C according to the DSC analyses. However, the other four PLM

images indicated that PTHF crystallization occurred under various levels of tensile strains.[26] Stain-induced polymer crystallization at room temperature was reported previously and was attributed to the strain-induced polymer chain alignment in the strain direction.[27-30] Stain-induced PTHF crystallization could possibly enhance the separation of the CNTs experiencing strain-induced alignment and reduce the electron tunneling efficiency among CNTs, thereby potentially contributing to the observed decrease in the electrical conductivity. To further confirm the strain-induced crystallization phenomenon, a series of XRD scans were performed on the nanocomposite films under various tensile strain conditions (Figs. 3c and d). As the tensile strain increased, two distinct diffraction peaks located at $2\theta = 19.9°$ and 24.4° were clearly observed corresponding to the (002) and (202) lattice planes of the PTHF crystalline structure, respectively.[2, 31] It was also found that the size of the PTHF crystallites increased with the tensile strain. For instance, when the tensile strain increased from 300% to 700%, according to the Scherrer equation as detailed in the Supporting Information,[32] the effective crystallite size of the PTHF increased from 2.57 to 4.48 nm and from 2.79 to 3.26 nm, respectively, based on the two diffraction peaks (002) and (202) located at 19.9° and 24.4°, respectively.[33] Conversely, these two sharp diffraction peaks gradually transformed into a broad peak after the tension was released, suggesting that the strain-induced PTHF crystallization was stain-dependent and is reversible. Therefore, while the piezoresistive effect exhibited by the CNT/ETC-PTHF nanocomposite is largely attributed to the strain-induced alignment of the CNTs causing a reduction in the connectivity of the CNT network,

strain-induced PTHF crystallization might also contribute to this effect (cf. Fig. 3e).

2.3 Detection of light poking and finger bending motions

In order to demonstrate the sensitivity of the CNT/ETC-PTHF nanocomposites for detecting weak mechanical stimuli, such as a light touch to human skin, a gentle poke test was carried out.[34] A piece of the 15 wt.% CNT/ETC-PTHF nanocomposite film was mounted between two clips and then the film was poked very gently using a plastic stick with a square contact surface (Fig. 4a). During the poke test, the electrical current through the film was measured with a bias of 5 V. As shown in Fig. 4b, the 15 wt.% CNT/ETC-PTHF nanocomposite provided a very quick and accurate response to the gentle poking motion. Once a poke was applied to the film, the current through the film dropped immediately. Likewise, once the poke was released from the film, the current recovered promptly. The ratio of current change ranged from 1.3% to 3.6% corresponding to a poke pressure ranging from 125 to 328 Pa, and the current responses of the nanocomposite film followed excellently with the cyclic poking stimuli. According to the literature,[36] the pressure of a mosquito landing on human skin varies between 800 to 3,266 Pa. This poke test proved that the CNT/ETC-PTHF nanocomposite was sensitive enough to detect weak stimuli; for example, weaker than the pressure of a mosquito landing.

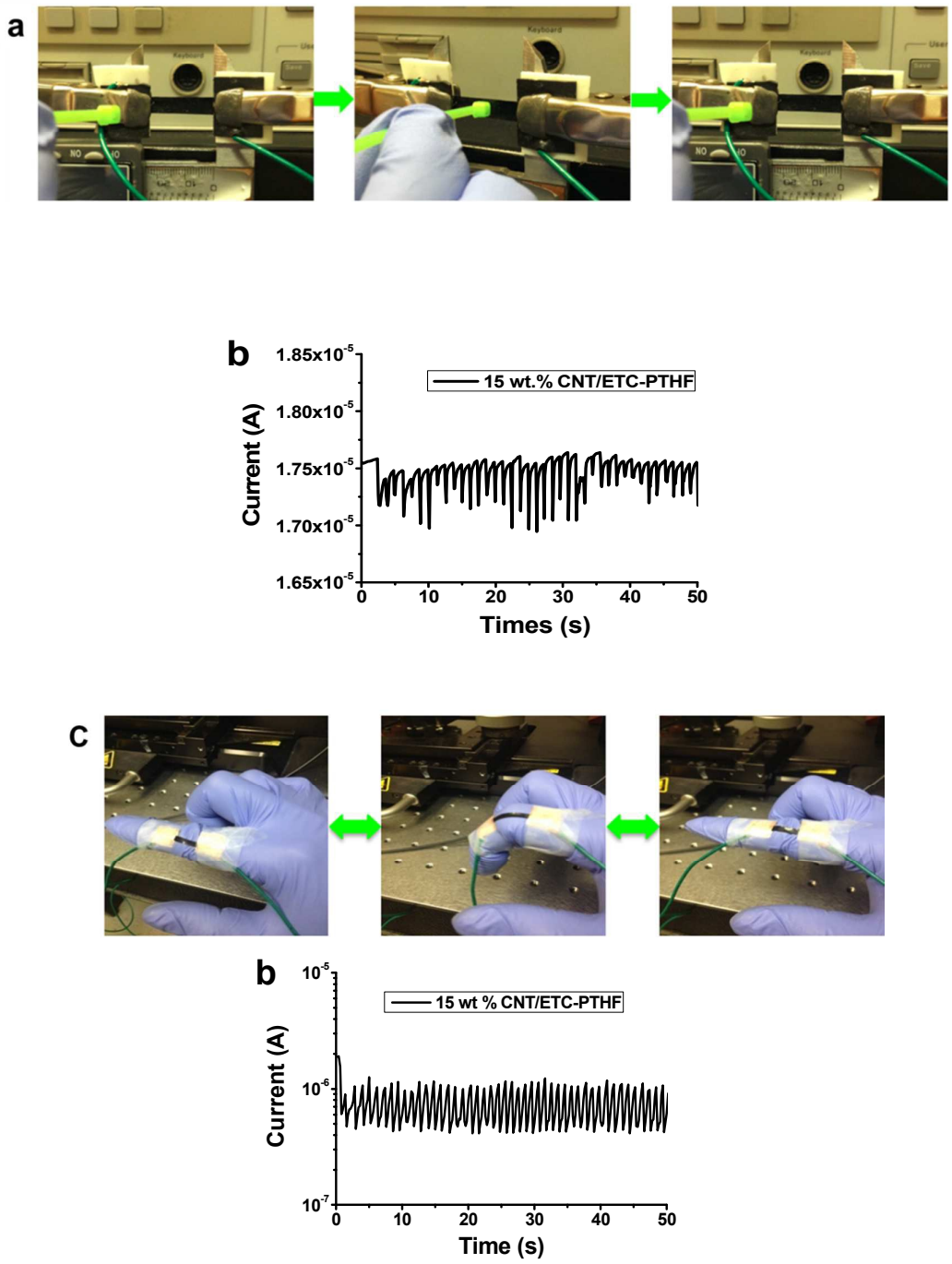

Fig. 4 (a) Optical images of each step of the poking motion (the pressure ranged from 125 to 328 Pa). (b) The electrical current response of the 15 wt.% CNT/ ETC-PTHF nanocomposite in the poking motion. (c) Optical images of each step of the bending finger movement.(d) The electrical current in the bending finger movement of the 15

wt.% CNT/ ETC-PTHF nanocomposite.

Since this family of CNT/ETC-PTHF nanocomposites is highly sensitive, stretchable, flexible, and human-friendly, they can be used as strain sensing materials for wearable and flexible human motion detection devices. The motion of the human body can reach a large strain ($\varepsilon > 50\%$) and bending angle ($\theta > 150^{o}$),[4] which needs to be accommodated by the motion sensors. In order to demonstrate the capability of our piezoresistive CNT/ETC-PTHF nanocomposite films for detecting the bending motion of human joints, a 15 wt.% CNT/ETC-PTHF nanocomposite film was mounted on a forefinger which underwent a straight-to-bend motion process (Fig. 4c). In this dynamic test, recurrent bending/relaxation cycles (with the bending angle ranging from 0 to 90^{o}) were applied to the index finger while the electrical current through the nanocomposite film was measured at a constant voltage bias of 5 V. As shown in Fig. 4d, the 15 wt.% CNT/ETC-PTHF nanocomposite responded to the bending motion with good sensitivity ($I_0/I = 4.61$) and could easily follow the quick motion of the finger (Supporting Information Video S1). The video shows that there was excellent agreement between the quick motion of the figure and the electrical current response of the CNT/ETC-PTHF nanocomposite film without apparent drifting or hysteresis. In comparison with previously reported data (e.g., a $\Delta R/R_0$ of approximately 10% and 30% in response to the index and middle finger motions, respectively),[37] the CNT/ETC-PTHF nanocomposite film had a $\Delta R/R0$ of 360% in response to the index finger bending motion, which was much more sensitive." This experiment confirms that the CNT/ETC-PTHF nanocomposite film exhibited a fast

response and an outstanding repeatability. Therefore, these nanocomposites could be used as an intelligent and accurate sensing material for various applications including biomechanics, kinesiology, and bionics.

The dielectric constant of the 15 wt.% CNT/ETC-PTHF nanocomposites as a function of the tensile strain was also measured at various frequencies ranging from 20 Hz to 2 MHz. As shown in Fig. S7, the dielectric constant decreased with increasing stretching strains. This finding suggests that the dielectric property of the CNT/ETC-PTHF nanocomposites can be regulated by an external strain[38]. Therefore, such materials may also be used for applications such as energy storage devices with mechanical-tunable dielectric properties.

3. Conclusions

A family of unique piezoresistive CNT/ETC-PTHF nanocomposites exhibiting high stretchability and high sensitivity as well as high stability to mechanical stimuli was developed using a simple and low cost fabrication process. The excellent piezo-resistive performance possessed by the CNT/ETC-PTHF nanocomposites may be contributed to the strain-induced CNT re-organization including uncoiling, disentanglement, and alignment of the CNTs. Stain-induced PTHF crystallization contributed to the observed piezoresistive effect. The piezoresistive CNT/ETC-PTHF nanocomposite films demonstrated significant and fast responses in electrical conductivity to joint bending and light poking motions, making them potentially

useful for various applications including electronic bionics skin, electronic textiles, and biomedical detectors.

4. Experimental Section

4.1 Synthesis of surface-functionalized CNTs

As shown in Scheme 1, CNTs were functionalized with 4-methoxyphenyl diazonium according to a method reported in the literature.[39] First, 4-methoxyphenyl diazonium was synthesized by dissolving 3 mmol p-anisidine in 20 mL DI water, followed by adding 0.75 mL of concentrated hydrochloric acid and 3 mmol sodium nitrite under constant stirring for 30 min. Then, 100 mg of CNTs and 10 mg of sodium dodecyl sulfonate (used as a surfactant) were dispersed in 100 mL of deionized water under sonication. Thereafter, the freshly made 4-methoxyphenyl diazonium solution was added to the CNT solution dropwise under sonication. The mixture was ultrasonicated at 300 W for 5 h at 50 °C, and then stirred overnight at ambient temperature. It was then filtered and washed in succession with water and ethanol. The resulting product—i.e., the functionalized CNTs—were dried overnight in a freeze-drier before use.

4.2 Synthesis of the highly elastomeric triisocyanate-crosslinked polytetrahydrofuran (ETC-PTHF)

Scheme 1 shows the synthesis route of the ETC-PTHF. The synthesis reaction

was conducted in dried glassware under an inert nitrogen (N_2) atmosphere. A mass of 2.9 g of dried PTHF (2.9 kDa), 245 mg TTI, and 3.0 mg dibutyltin dilaurate (DBT) were mixed in freshly distilled toluene and stirred for 6 h in an N_2 atmosphere at 25~30 °C to obtain highly elastomeric ETC-PTHF.

4.3 Synthesis of the CNT/ETC-PTHF nanocomposites

A specific amount of functionalized CNTs was dispersed in DMF via ultrasonication for one hour (Hielscher UP 400S, Bernau bei Berlin, Germany, 400 W). The resulting CNT solution and the ETC-PTHF toluene solution prepared earlier were ultrasonicated for 30 min at 60 °C to obtain a well-dispersed suspension. Subsequently, the functionalized CNT/ETC-PTHF solution was heated on a hot plate at 85 °C. The resulting CNT/ETC-PTHF nanocomposite film was further dried for 24 h at 80 °C under vacuum (0.0010 mBar).

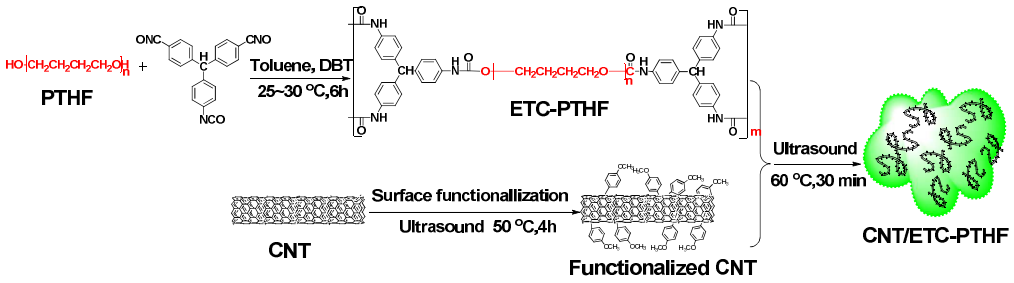

Scheme 1. The synthesis scheme of the surface-functionalized CNT, highly elastomeric ETC-PTHF, and CNT/ETC-PTHF nanocomposite films (thickness: 0.3~0.4 mm).

4.4 Characterization

The chemical structures of the CNTs, ETC-PTHF, and CNT/ETC-PTHF nanocomposites were analyzed using a Fourier transform infrared (FTIR) spectrophotometer (Bruker Tensor 27 FT-IR) at room temperature. The electrical conductivities of the nanocomposite films were measured using an HP4155 semiconductor analyzer. The two ends of the nanocomposite film were covered with silver paste serving as electrical contacts. The microstructure of the CNT/ETC-PTHF nanocomposite film was studied using a scanning electron microscope (LEO GEMINI 1530 SEM, Zeiss, Germany). Differential scanning calorimetry (DSC) analyses were performed in an N_2 atmosphere using a Q20 DSC thermal analyzer (TA Instruments, DE USA) from 0 to 100 °C at a heating rate of 5 °C/min. The thermal stability of these films were characterized via thermogravimetric analysis (TGA) using a TGA/Q50 thermal analyzer (TA Instruments, DE USA). Approximately 10 mg of the nanocomposite films were heated from 30 to 700 °C at a heating rate of 10 °C/min in an N_2 atmosphere. X-ray diffraction (XRD, Bruker D8-Discovery) analyses were carried out on the samples from 5° to 60° (diffraction angles, 2θ) under different strains. Polarized optical images of the crystalline ETC-PTHF were taken using a polarized light microscope (EN60950, Diagnostic Instruments Inc., MI, USA).

Acknowledgments

This work was partially supported by an AFOSR PECASE grant #FA9550-09-1-0482 and the University of Wisconsin–Madison. The AFOSR program manager is Dr. Gernot Pomrenke.

Competing Financial Interests

The authors declare no competing financial interests.

Notes and References

1. Park, S. et al. Stretchable energy-harvesting tactile electronic skin capable of differentiating multiple mechanical stimuli modes. *Adv Mater* **26**, 7324-32 (2014).
2. Rachmawati, R., Woortman, A.J. & Loos, K. Tunable properties of inclusion complexes between amylose and polytetrahydrofuran. *Macromol Biosci* **13**, 767-76 (2013).
3. Sekitani, T. et al. Stretchable active-matrix organic light-emitting diode display using printable elastic conductors. *Nat Mater* **8**, 494-9 (2009).
4. Amjadi, M., Pichitpajongkit, A., Lee, S., Ryu, S. & Park, I. Highly stretchable and sensitive strain sensor based on silver nanowire-elastomer nanocomposite. *ACS Nano* **8**, 5154-63 (2014).
5. Yao, S. & Zhu, Y. Wearable multifunctional sensors using printed stretchable conductors made of silver nanowires. *Nanoscale* **6**, 2345-52 (2014).
6. Lee, P. et al. Highly stretchable and highly conductive metal electrode by very long metal nanowire percolation network. *Adv Mater* **24**, 3326-32 (2012).
7. Wang, X., Hu, H., Shen, Y., Zhou, X. & Zheng, Z. Stretchable conductors with ultrahigh tensile strain and stable metallic conductance enabled by prestrained polyelectrolyte nanoplatforms. *Adv Mater* **23**, 3090-4 (2011).
8. Choong, C.L. et al. Highly stretchable resistive pressure sensors using a conductive elastomeric composite on a micropyramid array. *Adv Mater* **26**, 3451-8 (2014).
9. Kim, Y. et al. Stretchable nanoparticle conductors with self-organized conductive pathways. *Nature* **500**, 59-63 (2013).
10. Yao, S. & Zhu, Y. Nanomaterial-enabled stretchable conductors: strategies, materials and devices. *Adv Mater* **27**, 1480-511 (2015).
11. Tadakaluru, S., Thongsuwan, W. & Singjai, P. Stretchable and flexible high-strain sensors made using carbon nanotubes and graphite films on natural rubber. *Sensors (Basel)* **14**, 868-76 (2014).
12. Bae, S.H. et al. Graphene-based transparent strain sensor. *Carbon* **51**, 236-242 (2013).

13. Hou, Y. et al. Positive piezoresistive behavior of electrically conductive alkyl-functionalized graphene/polydimethylsilicone nanocomposites. *Journal of Materials Chemistry C* **1**, 515-521 (2013).
14. Yamada, T. et al. A stretchable carbon nanotube strain sensor for human-motion detection. *Nat Nanotechnol* **6**, 296-301 (2011).
15. Mehdi, S.M., Jo, J., Doh, Y.H., Dang, H.W. & Choi, K.H. Stretchable and Flexible Resistive Behavior of Poly(3,4-ethylenedioxythiophene): Poly(styrenesulfonate) Thin Film on Ultra-Low Modulus Polydimethylsiloxane with Trench-Type Roughness. *Journal of Polymer Science Part B-Polymer Physics* **53**, 226-233 (2015).
16. Guo, C.F., Sun, T., Liu, Q., Suo, Z. & Ren, Z. Highly stretchable and transparent nanomesh electrodes made by grain boundary lithography. *Nat Commun* **5**, 3121 (2014).
17. Amjadi, M. & Park, I. in Micro Electro Mechanical Systems (MEMS), 2015 28th IEEE International Conference on 744-747 (2015).
18. Sekitani, T. et al. A rubberlike stretchable active matrix using elastic conductors. *Science* **321**, 1468-72 (2008).
19. Georgousis, G. et al. Strain sensing in polymer/carbon nanotube composites by electrical resistance measurement. *Composites Part B-Engineering* **68**, 162-169 (2015).
20. Chen, Z. et al. Three-dimensional flexible and conductive interconnected graphene networks grown by chemical vapour deposition. *Nat Mater* **10**, 424-8 (2011).
21. Shin, M.K. et al. Elastomeric conductive composites based on carbon nanotube forests. *Adv Mater* **22**, 2663-7 (2010).
22. Kim, T.A., Kim, H.S., Lee, S.S. & Park, M. Single-walled carbon nanotube/silicone rubber composites for compliant electrodes. *Carbon* **50**, 444-449 (2012).
23. Lipomi, D.J. et al. Electronic Properties of Transparent Conductive Films of PEDOT:PSS on Stretchable Substrates. *Chemistry of Materials* **24**, 373-382 (2012).
24. Hbaieb, K., Wang, Q.X., Chia, Y.H.J. & Cotterell, B. Modelling stiffness of polymer/clay nanocomposites. *Polymer* **48**, 901-909 (2007).
25. Liu, Y. & Kumar, S. Polymer/carbon nanotube nano composite fibers--a review. *ACS Appl Mater Interfaces* **6**, 6069-87 (2014).
26. Gao, Y. et al. Stretching-induced interfacial crystalline structures and relevant mechanical properties in melt-spun polypropylene/whisker composite fibers. *Polymer* **53**, 2792-2801 (2012).
27. Zhang, W., Ning, N.Y., Gao, Y., Xu, F. & Fu, Q. Stretching induced interfacial crystallization and property enhancement of poly(L-lactide)/single-walled carbon nanotubes fibers. *Composites Science and Technology* **83**, 47-53 (2013).
28. Toki, S., Fujimaki, T. & Okuyama, M. Strain-induced crystallization of natural rubber as detected real-time by wide-angle X-ray diffraction technique.

Polymer **41**, 5423-5429 (2000).
29. Yin, Y.G. et al. Effect of nucleating agents on the strain-induced crystallization of poly(L-lactide). *Polymer* **65**, 223-232 (2015).
30. Meng, L.P. et al. Constrained and free uniaxial stretching induced crystallization of polyethylene film: A comparative study. *Polymer Testing* **36**, 110-118 (2014).
31. Rachmawati, R., Woortman, A.J., Kumar, K. & Loos, K. Inclusion Complexes Between Polytetrahydrofuran-b-Amylose Block Copolymers and Polytetrahydrofuran Chains. *Macromol Biosci* **15**, 812-28 (2015).
32. Lebovka, N.I. et al. Phase behaviour, microstructure, and percolation of poly(ethylene glycol) filled by multiwalled carbon nanotubes and organophilic montmorillonite. *Journal of Composite Materials* **45**, 2555-2566 (2011).
33. Liu, L.Z. & Chu, B. Crystalline structure and morphology of microphases in compatible mixtures of poly(tetrahydrofuran-methyl methacrylate) diblock copolymer and polytetrahydrofuran. *Journal of Polymer Science Part B-Polymer Physics* **37**, 779-792 (1999).
34. Roh, E., Hwang, B.-U., Kim, D., Kim, B.-Y. & Lee, N.-E. Stretchable, Transparent, Ultrasensitive, and Patchable Strain Sensor for Human–Machine Interfaces Comprising a Nanohybrid of Carbon Nanotubes and Conductive Elastomers. *ACS Nano* **9**, 6252-6261 (2015).
35. Zhang, W., Ning, N., Gao, Y., Xu, F. & Fu, Q. Stretching induced interfacial crystallization and property enhancement of poly(l-lactide)/single-walled carbon nanotubes fibers. *Composites Science and Technology* **83**, 47-53 (2013).
36. Kong, X.Q., Liu, J.L., Zhang, W.J. & Qu, Y.D. Load-bearing ability of the mosquito tarsus on water surfaces arising from its flexibility. *Aip Advances* **5** (2015).
37. Li, X.K., Gittleson, F., Carmo, M., Sekol, R.C. & Taylor, A.D. Scalable Fabrication of Multifunctional Freestanding Carbon Nanotube/Polymer Composite Thin Films for Energy Conversion. *Acs Nano* **6**, 1347-1356 (2012).
38. Balanis, C.A. Advanced engineering electromagnetics (John Wiley & Sons, Hoboken, N.J., 2012).
39. Park, J. & Yan, M. Covalent functionalization of graphene with reactive intermediates. *Acc Chem Res* **46**, 181-9 (2013).

Graphical Abstract

A family of CNT/ETC-PTHF nanocomposites exhibiting high stretchability and highly sensitivity to mechanical stimuli was developed. The electrical conductivity change of 15 wt.% CNT/ETC-PTHF nanocomposites can reach approximately 7.3%, 29.2%, 19.76, 169.2 and 1291 times when the tensile strain was 1%, 5%, 50%, 250%, and 500%, respectively.